AGU100 ADVANCING EARTH AND SPACE SCIENCE

Geophysical Research Letters

RESEARCH LETTER
10.1029/2018GL077229

Key Points:
- Consistent with DNS, microstructure data show $Ri_f \approx 0.2$ for $Re_B < O(100)$
- Consistent with DNS, covariance-derived fluxes show that Ri_f varies with Re_B for $Re_B > O(100)$
- Consideration of different studies shows that Ri_f in general depends on Re_B, but in a way that must depend on other parameters as well

Supporting Information:
- Supporting Information S1

Correspondence to:
S. G. Monismith,
monismith@stanford.edu

Citation:
Monismith, S. G., Koseff, J. R., & White, B. L. (2018). Mixing efficiency in the presence of stratification: When is it constant?. *Geophysical Research Letters*, *45*, 5627–5634. https://doi.org/10.1029/2018GL077229

Received 20 JAN 2018
Accepted 27 MAY 2018
Accepted article online 4 JUN 2018
Published online 14 JUN 2018

Mixing Efficiency in the Presence of Stratification: When Is It Constant?

Stephen G. Monismith[1], Jeffrey R. Koseff[1], and Brian L. White[2]

[1]Department of Civil and Environmental Engineering, Stanford University, Stanford, CA, USA, [2]Marine Sciences Department, University of North Carolina at Chapel Hill, Chapel Hill, NC, USA

Abstract The efficiency of the conversion of mechanical to potential energy, often expressed as the flux Richardson number, Ri_f, is an important determinant of vertical mixing in the ocean. To examine the dependence of Ri_f on the buoyancy Reynolds number, Re_B, we analyze three sets of data: microstructure profiler data for which mixing is inferred from rates of dissipation of turbulent kinetic energy (ε) and temperature variance (χ) measured in the open ocean, time series of spectrally fit values of ε and covariance-derived buoyancy fluxes measured in nearshore internal waves, and time series of spectrally fit values of ε and χ measured in an energetic estuarine flow. While profiler data are well represented by $Ri_f \approx 0.2$ for $1 < Re_B < 1{,}000$, the covariance data have much larger values of Re_B and, consistent with direct numerical simulation results, show that $Ri_f \sim Re_B^{-0.5}$. The estuarine data have values of Re_B that fall between those of the other two data sets but also shows $Ri_f \approx 0.2$ for $Re_B < 5000$. Overall, these data suggest that Ri_f is in general not constant and may be substantially less than 0.2 when Re_B is large, although the value at which the transition from constant to Re_B-dependent mixing may depend on additional parameters that are yet to be determined. Nonetheless, for much of the ocean, $Re_B < 100$ and so Ri_f is constant there.

Plain Language Summary The efficiency of turbulent mixing, the rate at which mechanical energy of turbulence is converted into changes in potential energy, plays a central role in determining the dynamics of ocean circulation and the transport of carbon. This efficiency is commonly assumed to be constant, although there is evidence that it can depend on the strength of the turbulence, measured by the rate of dissipation of the turbulence energy, and the strength of the density stratification. Notably, ocean circulation models with variable efficiency produce different flows than do ones with constant efficiency. Using three oceanic data sets, including the large body of microstructure data acquired over the past 20 years, we analyze how efficiency varies with turbulence strength. Consideration of these data, and other published data, shows that mixing efficiency is, as commonly assumed, likely to be constant in much of the ocean. In contrast, in places that are highly turbulent, for example, very energetic currents, it might be relatively low. We show that at present, what controls the transition from constant to variable efficiency remains uncertain, although reanalysis of existing microstructure data in energetic parts of the ocean should help clarify the extent to which mixing efficiency varies in these regions.

1. Introduction

Turbulent mixing in the ocean is strongly affected by density stratification (Turner, 1973), behavior that is important to controlling distributions of water properties as well as functioning of many marine ecosystems. The extent to which turbulent mixing is affected by stratification can be represented by the flux Richardson number, Ri_f, defined by Ivey and Imberger (1991) as

$$Ri_f = \frac{B}{B + \varepsilon} \tag{1}$$

where B is the turbulent buoyancy flux and ε is the rate of dissipation of turbulent kinetic energy (TKE). Equation (1) generalizes Turner's (1973) definition for which $B + \varepsilon$ is replaced by the rate of TKE production, P. In steady, homogeneous turbulence $P = B + \varepsilon$, whereas more generally $B + \varepsilon$ represents the net supply of TKE including P, vertical divergence of TKE flux, and the rate of change of TKE with time.

Equation (1) is advantageous in that ε can be estimated with shear profilers (see, e.g., Gregg et al., 2018), and B can be computed from estimates of χ, the rate of dissipation of temperature variance, as

$$B; \left(\frac{\partial T}{\partial z}\right)^{-2} \frac{\chi}{2} N^2 \tag{2}$$

where N is the buoyancy frequency and T is the depth (z)-variable mean density profile (Osborn & Cox, 1972). Additionally, B defined by equation (2) is a good estimate of mixing efficiency because it measures irreversible mixing as opposed to covariance-based values of B, which can include both reversible and irreversible processes (Caulfield & Peltier, 2000). Nonetheless, for the most part, following Osborn (1980), microstructure-based measurements of ocean mixing have assumed that $Ri_f = 0.17$ and computed mixing rates solely from measurements of ε, although Osborn carefully argues that 0.17 is only an upper bound on Ri_f.

Gregg et al. (2018) argue that because estimates of vertical mixing based on $Ri_f = 0.17$ do not differ significantly from values inferred from tracer dispersion (e.g., Ruddick et al., 1997), "… observations should continue to be scaled with [0.17] until observations, laboratory experiments, and numerical simulations converge on a more accurate formulation." However, this view overlooks the body of evidence that shows that Ri_f can be substantially less than 0.17 when turbulence is energetic and stratification is weak. The direct numerical simulations (DNSs) of stratified shear flows reported in Shih et al. (2005), as well as laboratory experiments (Barry et al., 2001), microstructure profiling (Bouffard & Boegman, 2013), and direct measurements of B in nearshore breaking internal waves (Davis & Monismith, 2011; Walter et al., 2014), show relationships of the form:

$$Ri_f = C\ \mathrm{Re}_B^{-1/2} \tag{3}$$

where the buoyancy Reynolds number, Re_B, is defined as (Gibson, 1980)

$$\mathrm{Re}_B = \frac{\varepsilon}{\nu \mathrm{N}^2} \tag{4}$$

when $Re_B > \mathrm{O}(100)$. C varies from 1.5 (Shih et al., 2005) to 4 (Bouffard & Boegman, 2013). When $Re_B < \mathrm{O}(100)$, Ri_f is found to be a constant ≤ 0.25. As noted by de Lavergne et al. (2016) and Mashayek et al. (2017), a dependence of Ri_f on Re_B of this type may be significant in determining the importance of internal wave breaking to the general circulation. Nonetheless, not all data taken with large values of Re_B obey equation (3). In particular, estimates of Ri_f reported by Holleman et al. (2016) for an energetic estuarine flow (median $Re_B \approx 2{,}000$) have a median value of $Ri_f = 0.21$.

Motivated by the differences between the results cited by Gregg et al. (2018) showing $Ri_f \approx 0.17$, and the various experiments and observations that show Ri_f (Re_B), we examined the constancy of Ri_f using the Scripps Institute of Oceanography database of microstructure profiler observations (Waterhouse et al., 2014). In this database there are eight data sets that include both ε and χ, and so can be used to compute Ri_f. As we will show below, these data, which mostly have $Re_B < \mathrm{O}(100)$, strongly support the contention that in general Ri_f is constant. In contrast, a composite of four data sets in which buoyancy fluxes were measured directly and for which Ri_f (Re_B) follows equation (3) is characterized by much higher values of Re_B ($\mathrm{O}(10^4)$) and much smaller values of Ri_f ($\mathrm{O}(0.01)$).

2. Methods

The microstructure profiler data we use come from the National Science Foundation-supported microstructure database curated by Dr. Amy Waterhouse and Prof. Jennifer McKinnon (https://microstructure.ucsd.edu). Specifically, we use profiles of salinity, temperature, ε, and χ taken in studies of mixing below the thermocline reported at either 0.5- or 1-m intervals. Eight of the data sets in the archive have all four variables (see Table 1). N^2 was computed from salinity and temperature using the EOS 80 Seawater toolbox, and the adiabatic leveling method of Bray and Fofonoff (1981), as recommended by the Microstructure working group (A. Waterhouse, personal communication, 2017). Points with $N^2 \leq 0$ were excluded from further analysis. Also, based on the work of St. Laurent and Schmitt (1999), to avoid regions in which double diffusion may be active, only points with $0.5 < R_\rho < 2$ where $R_\rho = \alpha(dT/dz)/\beta(dS/dz)$, were used. These raw data were then averaged over 10 m using a moving average. B was computed using equation (2).

The second data set is a set of four studies of stratified nearshore flows that involved direct measurements of B via measurement of covariance of fluctuating densities and vertical velocities using acoustic Doppler velocimeters and conductivity and temperature sensors, and ε via inertial subrange fitting of vertical velocity spectra, both computed using 10-min averaging periods. The measurement protocols are described in

Table 1
Mixing Data Sets

Data set	Study	Re_B[a]	Ri_f[b]	Segments[c]	Data source/PI
Microstructure	NATRE	18	0.2	31,248	K. Polzin
	BBTRE96/97	49	0.17	36,421	K.Polzin, L. St. Laurent, J. Toole
	SPAM1/2	8.9	0.27	26,781	G. Carter
	MIXET2	1.2	0.65	2281	G. Carter
	EXITS1	8.6	0.14	464	G. Carter
	GRAVILUCK	107	0.19	2529	L. St. Laurent and A. Thurnherr
Covariance	Various (see references in text)	9330	0.015	2,594	S. Monismith
Estuarine	Holleman et al. (2016)	1840	0.21	994	R. Holleman and W. R. Geyer

[a]Values of Re_B. [b]Ri_f shown are median values for each data set. [c]For microstructure data, "segments" refers to 10 m bins in vertical profiles; for covariance data, segments refers to 10-min averaging periods; and for estuarine data, segments refers 20-s averaging periods, which represent ~30 m in the streamwise direction.

details in Davis and Monismith (2011) and Walter et al. (2014), where results for flow dynamics, mixing, etc., are also given. In addition to these two data sets, we also include two other similar data sets, the first from internal tides propagating over a Red Sea coral reef (Dunckley, 2012) and the second from shoaling internal tides in Mamala Bay (Squibb, 2014). Instrumentation and data processing used in these latter two studies were identical to those used in Davis and Monismith (2011) and Walter et al. (2014). In all cases errors in estimation of ε and B were generally less than 27% and 57%, respectively, for any single averaging period, giving a maximum uncertainty in any single value of Ri_f of 60%; that is, Ri_f was between 40% and 160% of the measured value (Davis & Monismith, 2011), while relatively large, this is still smaller than the scatter in Ri_f shown below for the covariance data. To eliminate possible variability associated with small values of N^2 (cf. Gregg et al., 2018], data with $N^2 < 2 \times 10^{-5}$ s^{-2} (corresponding to $dT/dz \sim 0.01$°/m) were excluded from the analysis we present here. It is important to note that in all four cases, Ri_f can be fit with equation (3). Detailed analysis of these four data sets will be presented elsewhere.

A third data set that we consider is that of Holleman et al. (2016), who measured both ε and χ in a strongly sheared and stratified estuarine flow using an array of acoustic Doppler velocimeters and conductivity and temperature sensors deployed from a moving boat. Holleman et al. determined ε and χ using spectral fitting, and B was then computed using equation (2).

3. Results

The microstructure profiler data shown in Table 1 represent approximately 100,000 segments falling primarily in the ranges $0.1 < Re_B < 10^4$ and $10^{-3} < Ri_f < 1$ (Figures 1a and 1c). The bulk of the data come from NATRE (Toole et al., 1994), from the two Brazil Tracer Release programs (St. Laurent et al., 2001) and from the Samoan Passage programs (Alford et al., 2013). Remarkably, binning the data by Re_B shows that for $Re_B > 10$, approximately where one may expect a transition from internal waves to active turbulence (Gibson, 1980), the median value of $Ri_f \approx 0.17$, as first suggested by Osborn (1980), and as found by Shih et al. (2005) for $10 < Re_B < 60$. The confidence intervals determined by bootstrapping (Efron & Tibshirani, 1993; not shown) are essentially zero, except at the largest values of Re_B, where there are few points. Surprisingly, Ri_f increases with decreasing Re_B when $Re_B < 10$, reaching a maximum of nearly $Ri_f \approx 0.7$ when $Re_B \approx 0.1$. As seen in the laboratory experiments of Davies Wykes and Dalziel (2014), this value of Ri_f has been shown to be nearly maximal and is typically found for turbulence produced by convection. It is possible that this result is an experimental artifact since these low values of Re_B correspond to small values of ε and χ, which may not be well resolved by the profiler sensors (Polzin & Montgomery, 1998), or because the flow is undergoing transition to turbulence (Smyth et al., 2001). More generally, flows with $Re_B < 1$ are not likely turbulent (Brethouwer et al., 2007) and so data with $Re_B < 1$ may not properly represent vertical mixing. Likewise, for large values of Re_B, ε and χ may be under-resolved because the shear probe and thermistor spatial resolutions are larger than the Kolmogorov and Batchelor scales, respectively.

The distributions of Re_B and Ri_f can be examined in more details by plotting histograms of the data (Figures 1b and 1c). Given that both variables vary over multiple decades, examination of the distributions of logarithms is appropriate. Here too, a second remarkable feature of the profiler data set emerges: both

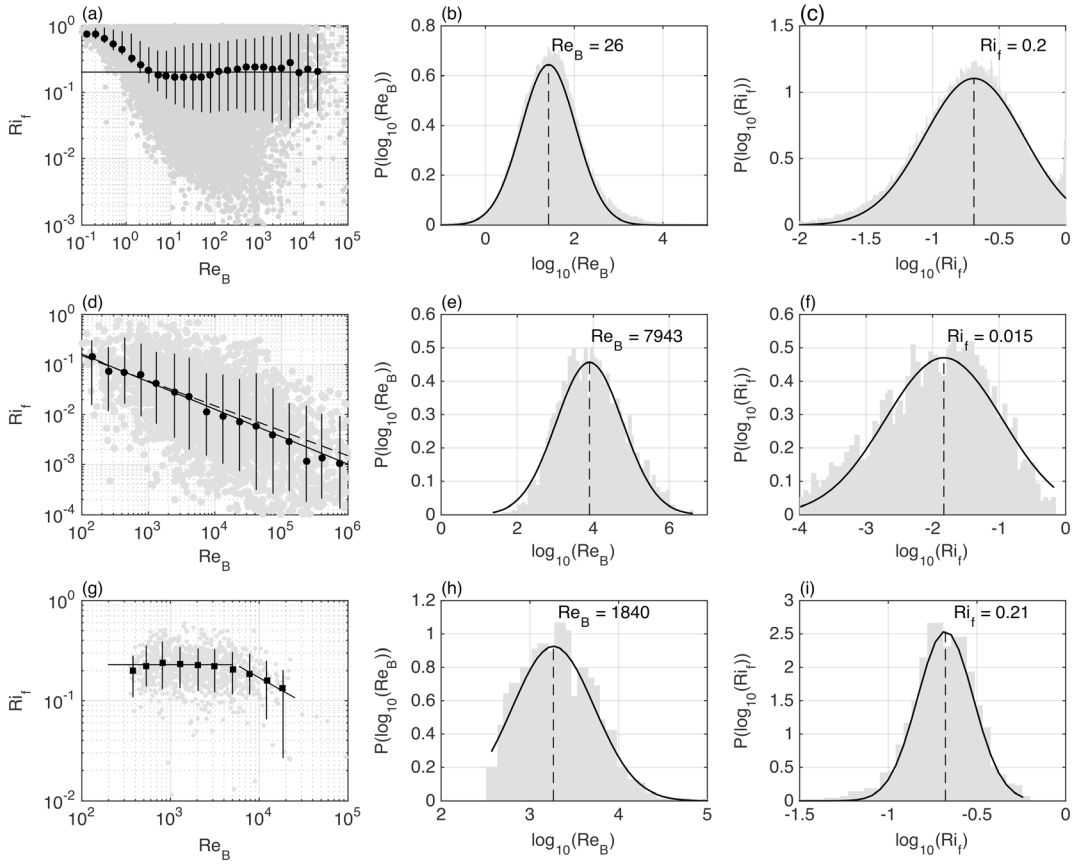

Figure 1. Ri_f and Re_B for three turbulent mixing data sets. Ri_f as a function of Re_B is given for (a) microstructure profiler data, (d) covariance data, and (g) estuarine data of Holleman et al. (2016). The closed symbols represent median values of Ri_f with error bars showing 10th and 90th percentiles of the data in each bin. The solid lines represent fits to the binned data, whereas the dashed line in (d) is the relation found by Shih et al. (2005). Histograms of (b, e, and h) Re_B and (c, f, and i) Ri_f are also given for the same three data sets. In each of these panels the solid lines show least squares fits to lognormal distributions with histograms and fits are scaled so that the integral of the lognormal fitted pdf is 1.

Ri_f and Re_B are distributed lognormally, despite good reasons to believe that this should not be the case (Yamazaki & Lueck, 1990). This lognormality holds for each of the data sets individually (see the supporting information) and also is seen in the float data presented by Salehipour et al. (2016). As seen in Figure 3, the median value of $Re_B = 26$ (Salehipour et al. find $Re_B \approx 30$), and the median value of $Ri_f = 0.2$, behavior that is consistent with the results of Shih et al. (2005) for $Re_B < 60$.

The results of the four covariance data sets paint a somewhat different picture. These data are characterized by a clear dependence on Re_B, much large values of Re_B, that is, $100 < Re_B < 10^6$, and somewhat smaller values of Ri_f, that is, $10^{-5} < Ri_f < 1$ (Figures 1d and 1f). Least squares fitting of Ri_f binned by quarter decades of Re_B shows that $Ri_f = 2\ Re_B^{-0.55}$ ($r^2 = 0.96$), which is remarkably close to the Shih et al. (2005) relation (Figure 1d). These data also show the lognormality seen in the profiler data, with the median value of $Re_B = 7943$ and the median value of $Ri_f = 0.015$. Thus, the covariance data set describes much more energetic turbulence than does the profiler data, and, consistent with the results of Shih et al. (2005), has much lower mixing efficiencies.

In contrast, the estuarine data set of Holleman et al. (2016) has $Ri_f \approx$ constant for somewhat higher values of Re_B than does the covariance data set (Figure 1g), although there is also a decrease of Ri_f with Re_B for $Re_B > 5{,}000$. These data have a range of values of Re_B that lie between those of the profiler data sets and those of the covariance data sets (Figure 1h). Like the other data, the probability density function of Re_B is well described by the lognormal distribution. Agreeing well with the profiler data (but not the covariance data), the median value of the estuarine data is $Ri_f = 0.21$, and, as seen with the two other data sets, is distributed lognormally (Figure 1i).

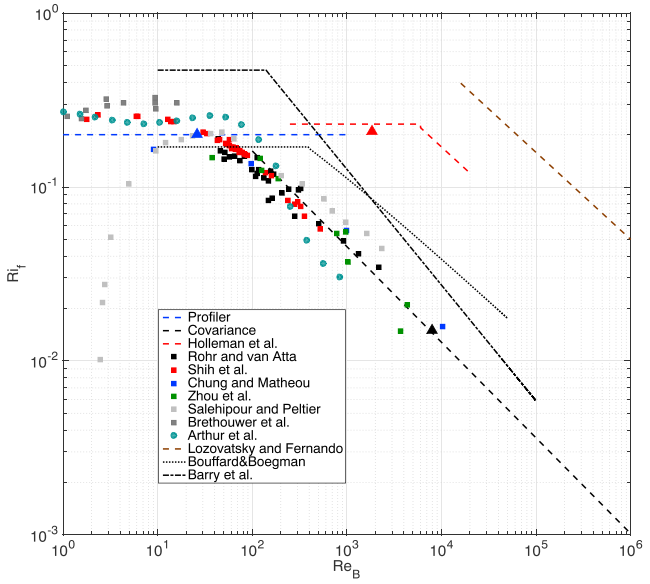

Figure 2. Schematic of different observations of Ri_f and Re_B. Symbols as given in the legend. Curves for "Profiler," "Covariance," and "Holleman et al" represent the fits and Re_B ranges seen in Figure 1, with the large triangles showing the median values of Ri_f and Re_B for each of these three data sets. Other field data are from Lozovatsky and Fernando (2013) (atmospheric boundary layer) and Bouffard and Boegman (2013). DNS data are from Shih et al. (2005), Chung and Matheou (2012), Zhou et al. (2017), Salehipour and Peltier (2015), Brethouwer et al. (2007), and Arthur et al. (2017). Lab data for homogeneous shear are from Rohr and van Atta (1987), and for homogeneous un sheared, stirred turbulence from Barry et al. (2001).

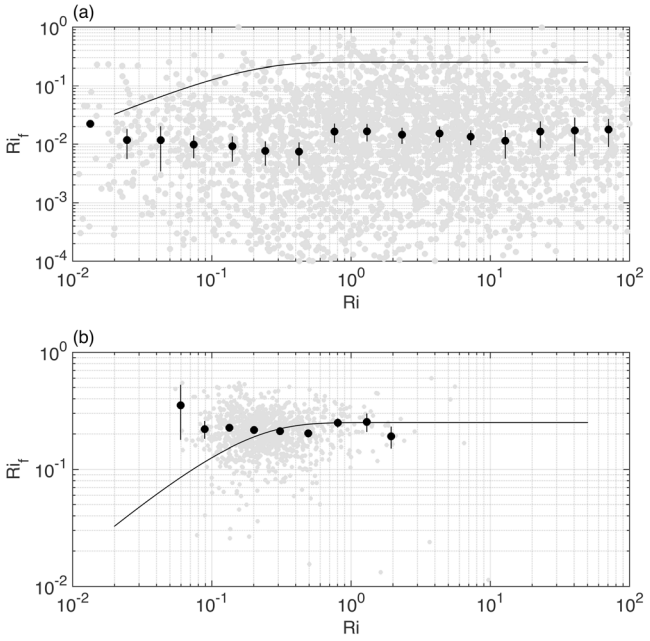

Figure 3. Ri_f as a function of Ri for (a) covariance data and (b) estuarine data of Holleman et al. (2016). The closed symbols are quarter-decade bin averages with error bars determined by bootstrapping. The solid line in each figure is the formula given by Vennaygamoorthy and Koseff (2016): $Ri_f = 0.25(1 - \exp[-7Ri])$.

Holleman et al. (2016) argued that the reduced values of Ri_f at large values of Re_B seen in their data were an effect of boundary proximity (see also Scotti & White, 2016). However, the reduction in Ri_f at large Re_B appears to reflect the fact that the highest values of Re_B coincide with smallest values of (z/L_O), for z the height above the bed and $L_O = (\varepsilon/N^3)^{0.5}$ the Ozmidov length (Turner, 1973). Indeed, for values of Re_B where there are data with both $(z/L_O) < 10$ or > 10 (the cutoff used by Holleman et al.), Ri_f does not appear to depend on (z/L_O) (see the supporting information). These two points also hold for the covariance data (see the supporting information). Large values of Re_B mostly occur for small values of (z/L_O), and Ri_f (Re_B) tends to not depend separately on (z/L_O). It should be noted that the two data sets have somewhat different values of (z/L_O): For the Holleman et al. data $1 < (z/L_O) < 50$ with a median value of 9, whereas for the covariance data, $0.05 < (z/L_O) < 100$ with a median value of 3.8. In both cases, the issue is that L_O and Re_B involve the same variables (ε and N^2) and so are themselves well correlated.

4. Discussion

From the standpoint of statistical averages, it is clear that much of the ocean below the mixed layer, at least as far as it has been sampled by microstructure profilers, and, as argued by Gregg et al. (2018), is well characterized by $Ri_f = 0.2$, albeit with substantial variability. Given that a majority of these data have $10 < Re_B < 100$, the regime where Ri_f is expected to be constant, this result is consistent with the findings of Shih et al. (2005) as well as others (e.g., Barry et al., 2001). In contrast, the covariance data all have $Re_B > 100$, and, per Shih et al. (2005), fall in the regime described by equation (3) and so Ri_f should be substantially less than 0.2, as observed.

For $Re_B > 100$, the covariance data appear to agree closely with the DNS results for homogeneous shear of Shih et al. (2005) and Chung and Matheou (2012); the DNS of Kelvin-Helmholtz instabilities of Salehipour and Peltier (2015); the DNS of stratified Couette flow reported by Zhou et al. (2017), albeit only in the center of their channel; and laboratory results for stratified, homogeneous stratified shear flows given by Rohr and van Atta (1987), that is, as seen in their Figure 7a. Moreover, countering the concern of various authors (e.g., Gregg et al., 2018) that the Shih et al. DNS results are affected by numerical artifacts, Figure 2 shows that the Rohr and van Atta experimental data, for which the length scales are not limited by the channel size nor are the smallest scales under-resolved, are remarkably close to the DNS results of Shih et al. Thus, it is clear that the Shih et al. results represent the steady, homogeneous shear limit of mixing by stratified turbulence and that the turbulence seen in the four covariance data sets appears to conform best to the dynamics of this limiting flow case.

The Holleman et al. (2016) data for Ri_f also make a transition to a dependence on Re_B, albeit at a much higher value of Re_B than what is seen in any of the other lab or oceanic data sets, that is, 70 (Shih et al., 2005), 200 (Barry et al., 2001), and 400 (Bouffard & Boegman, 2013). Moreover, stable atmospheric boundary layers (SABL) that satisfy Monin-Obukhov scaling (e.g., Grachev et al., 2015) do not show a unique relationship of the form $Ri_f = f(Re_B)$, although any individual

data set might show such a relation (Scotti & White, 2016). Indeed, the SABL data of Lozovatsky and Fernando (2013) do satisfy equation (3), except that the constant of proportionality C is much larger than values seen in DNS and oceanic studies.

There is no reason to believe that any of the different data sets have methodological biases that would explain why they differ. Thus, as argued by Scotti and White (2016) and Gregg et al. (2018), Ri_f cannot depend *only* on Re_B. Indeed, Salehipour et al. (2016) follow this approach and choose $Ri_f = g\,(Ri, Re_B)$, where the gradient Richardson number $Ri = N^2/S^2$. As seen in Figure 3, neither the covariance nor the estuarine data appear to depend systematically on Ri. In particular, they do not match the function $Ri_f\,(Ri)$ described in Vennaygamoorthy and Koseff (2016), a function that fits *both* the Shih et al. (2005) DNS data and the SABL data of Lozovatsky and Fernando (2013) reasonably well. Unfortunately, the microstructure database does not include values of Ri, so no conclusions can be drawn as to its importance for the profiler data. On the other hand, it is striking that the covariance data include a much wider range of values of Ri (0.01 to 100) than does the Shih et al. DNS (0.16 to 1) yet $Ri_f\,(Re_B)$ is nearly identical in the two cases.

More generally, depending on which other dimensional variables are thought to be important, for example, S, the Buckingham Pi theorem (e.g., Street et al., 1996) specifies the number of dimensionless variables that may serve to define Ri_f. That is, if there are n variables, which likely would only have units of meters and seconds, Ri_f could at most depend on $(n-3)$ dimensionless variables. Thus, if the only relevant variables are B, ε, ν, and N^2, then Ri_f must be only a function of Re_B. If S, TKE, k, and turbulent length scale l_t are also thought to be important, then three other parameters upon which Ri_f could depend would be Ri, the Froude number $Fr_k = \varepsilon/Nk$ (Maffioli et al., 2016), and $Fr_t = (L_O/L_t)^{2/3}$ (Ivey & Imberger, 1991). We note that few data sets include S and fewer still include k; neither is reported in the microstructure database. However, the covariance data set also differs significantly in Fr_k values from those of Shih et al. (2005), so would produce different $Ri_f\,(Fr_k)$ functional relationships (not shown), suggesting that $Ri_f\,(Fr_k)$ is not likely to be universal either. If L_t is taken to be the Thorpe scale, the length scale of overturns seen in profiles, it could be calculated from microstructure data, although for weak stratification, it could be highly dependent on sensor noise. This would be worth exploring in the future, especially given that the Thorpe scale and the Ellison scale, the scale defined by time series of the fluctuating density (Ivey et al. 2018), are closely correlated, thus facilitating comparable analysis of both types of data.

Finally, L_t could be assumed to be proportional to the height, z, above a solid boundary, as in Monin-Obukhov theory (Grachev et al., 2015), although as seen above, neither of the two data sets for which z/L_O was available could dependence of Ri_f on z/L_O be differentiated from dependence on Re_B. In any case, it is possible that Ri_f is dependent on more than local, instantaneous conditions; for example, besides parameters like Re_B, Ri_f may also depend on how the given flow was established or is maintained (Mashayek et al., 2017).

The difference between $Ri_f = 0.2$ and $Ri_f \approx 2\,Re_B^{-0.5}$ (taking an approximate average of the various values of C in equation (3) from the various published studies) can be significant when Re_B is large. For example, microstructure data reported by Mead Silvester et al. (2014) in the Antarctic Circumpolar Current have $Re_B = 0(10^6)$ (T. Rippeth, personal communication, 2017) implying values of Ri_f that would be 100 times smaller than the value of 0.2 seen in much of the profiler data. Unfortunately, χ is not likely to be resolved directly in energetic regions like this or in bottom boundary layers like that studied by Nash et al. (2004). However, the method described by Bluteau et al. (2017) in which χ is determined from profiler data by fitting of temperature and salinity variations may be a useful way of inferring χ, and thus for inferring B for portions of the ocean for which χ cannot be measured directly. Indeed, it appears that at present, the best way forward would be to apply the approach of Bluteau et al. to existing data sets from energetic parts of the ocean where Re_B is large, for example, bottom boundary layers (Nash et al. (2004) or strong current systems (Mead Silvester et al., 2014).

The profiler data, as well as all of the DNS results shown in Figure 2, including DNS studies of stirred stratified turbulence by Brethouwer et al. (2007) and of breaking internal waves by Arthur et al. (2017), and excepting those of Salehipour and Peltier (2015), show constancy of Ri_f for $1 < Re_B < 10$, a regime where the irreversible mixing can differ considerably from the covariance-based buoyancy flux (Vennaygamoorthy & Koseff, 2016). A nonzero Ri_f is unexpected given that $B \approx 0$ might be expected for these conditions. The behavior for Salehipour and Peltier's results for $Re_B < 10$ may reflect the fact that Ri_f and Re_B were computed using

volume averages, which can differ from averages calculated with local values of N, etc. (cf. Arthur et al., 2017). In any case, the small Re_B regime clearly deserves further attention.

5. Conclusions

We agree with the assertion of Gregg et al. (2018) that this issue of constancy or variability of Ri_f is not settled. However, examination of data not considered by Gregg et al. shows that there is clear evidence that Ri_f can vary with Re_B such that Ri_f is small when Re_B is large in the fashion described by Shih et al. (2005). Indeed, the general structure of $Ri_f(Re_B)$ that emerges from presently available data is one in which $Ri_f(Re_B)$ has a constant portion for Re_B less than some transitional value and then decays approximately like ${Re_B}^{-1/2}$ for larger values of Re_B. At a minimum, all the data sets agree that $Ri_f \approx 0.2$ for $Re_B < \mathrm{O}(100)$. In agreement with Shih et al., the covariance data sets show the $Ri_f \sim {Re_B}^{-0.5}$ for $Re_B > 100$, whereas the estuarine data of Holleman et al. (2016) show a transition to $Ri_f \sim {Re_B}^{-0.5}$ near $Re_B \approx 5{,}000$. Overall, these results suggest that while Ri_f is not constant and does depend on Re_B, it does not *uniquely* depend of Re_B. In terms of inferring mixing from dissipation data in energetic portions of the ocean, it remains to be determined what sets the value of Re_B for the transition from constant Ri_f to a functional relationship of the form $Ri_f \sim {Re_B}^{-1/2}$ occurs. Nonetheless, for much of the ocean interior $Re_B < 100$ and so Ri_f is constant there.

Acknowledgments

S. G. M. thanks the Stratified Turbulence group at Cambridge University, Tom Rippeth, and Geno Pawlak for discussions of this topic; Amy Waterhouse, who supplied guidance on use of the microstructure database; and Rusty Holleman, who provided the estuarine data. The covariance data were collected and analyzed by Ryan Walter, Brock Woodson, Mike Squibb, Jamie Dunckley, and Kristen Davis. The authors are especially grateful to those who collected and analyzed the microstructure data we used: K. Polzin, J. Toole, R. Schmidt, L. St. Laurent, G. Carter, M. Alford, and A. Thurnherr. B. L. W. was supported by a UPS Visiting Professorship and NSF grant OCE-1736989. The covariance data can be found at https://doi.org/10.5281/zenodo.1209410, and the estuarine data can be found at https://doi.org/10.5281/zenodo.1209425.

References

Alford, M. H., Girton, J. B., Voet, G., Carter, G. S., Mickett, J. B., & Klymak, J. M. (2013). Turbulent mixing and hydraulic control of abyssal water in the Samoan Passage. *Geophysical Research Letters*, *40*, 4668–4674. https://doi.org/10.1002/grl.50684

Arthur, R. S., Venayagamoorthy, S. K., Koseff, J. R., & Fringer, O. B. (2017). How we compute N matters to estimates of mixing in stratified flows. *Journal of Fluid Mechanics*, *832*(R2), 1–10.

Barry, M. E., Ivey, G. N., Winters, K. B., & Imberger, J. (2001). Measurements of diapycnal diffusivities in stratified fluids. *Journal of Fluid Mechanics*, *442*, 267–291.

Bluteau, C. E., Lueck, R. G., Ivey, G. N., Book, J. W., & Rice, A. E. (2017). Determining mixing rates from concurrent temperature and two velocity measurements. *Journal of Atmospheric and Oceanic Technology*, *34*(10), 2283–2293. https://doi.org/10.1175/JTECH-D-16-0250.1

Bouffard, D., & Boegman, L. (2013). A diapycnal diffusivity model for stratified environmental flows. *Dynamics of Atmospheres and Oceans*, *61-62*, 14–34. https://doi.org/10.1016/j.dynatmoce.2013.02.002

Bray, N. A., & Fofonoff, N. P. (1981). Available potential energy for MODE eddies. *Journal of Physical Oceanography*, *11*(1), 30–47. https://doi.org/10.1175/1520-0485(1981)011%3C0030:APEFME%3E2.0.CO;2

Brethouwer, G., Billant, P., & Chomaz, J. M. (2007). Scaling analysis and simulation of strongly stratified turbulent flows. *Journal of Fluid Mechanics*, *585*, 343–368. https://doi.org/10.1017/S0022112007006854

Caulfield, C. P., & Peltier, W. R. (2000). Anatomy of the mixing transition in homogeneous and stratified free shear layers. *Journal of Fluid Mechanics*, *413*, 1–47.

Chung, D., & Matheou, G. (2012). Direct numerical simulation of stationary homogeneous stratifed sheared turbulence. *Journal of Fluid Mechanics*, *696*, 434–467.

Davies Wykes, M. S., & Dalziel, S. B. (2014). Efficient mixing in stratified flows: Experimental study of a Rayleigh–Taylor unstable interface within an otherwise stable stratification. *Journal of Fluid Mechanics*, *756*, 1027–1057. https://doi.org/10.1017/jfm.2014.308

Davis, K. A., & Monismith, S. G. (2011). The modification of bottom boundary layer turbulence and mixing by internal waves shoaling on a barrier reef. *Journal of Physical Oceanography*, *41*(11), 2223–2241. https://doi.org/10.1175/2011JPO4344.1

de Lavergne, C., Madec, G., Le Sommer, J., Nurser, G. A. J., & Naveira Garabato, A. C. (2016). On the consumption of Antarctic Bottom Water in the abyssal ocean. *Journal of Physical Oceanography*, *46*(2), 635–661. https://doi.org/10.1175/JPO-D-14-0201.1

Dunckley, J. F. (2012). Mixing in nearshore coastal environments, (PhD thesis). (200 pp.). Department of Civil and Environmental Engineering, Stanford University.

Efron, B., & Tibshirani, R. (1993). *Introduction to the Bootstrap*. New York, NY: Chapman Hall. https://doi.org/10.1007/978-1-4899-4541-9

Gibson, C. H. (1980). Fossil temperature, salinity, and vorticity turbulence in the ocean. In J. C. Nihoul (Ed.), *Marine Turbulence Proceedings of the 11th International Liege Colloquium on Ocean Hydrodynamics*, *Elsevier Oceanography Series* (Vol. 28, pp. 221–257). New York, NY: Elsevier/North-Holland Inc. https://doi.org/10.1016/S0422-9894(08)71223-6

Grachev, A., Andreas, E., Fairall, C., Guest, P., & Persson, P. (2015). Similarity theory based on the Dougherty–Ozmidov length scale. *Quarterly Journal of the Royal Meteorological Society*, *141*(690), 1845–1856. https://doi.org/10.1002/qj.2488

Gregg, M. C., D'Asaro, E. A., Riley, J. J., & Kunze, E. (2018). Mixing efficiency in the ocean. *Annual Review of Marine Science*, *10*, 9.1–9.31.

Holleman, R. C., Geyer, W. R., & Ralston, D. K. (2016). Stratified turbulence and mixing efficiency in a salt wedge. *Journal of Physical Oceanography*, *46*(6), 1769–1783. https://doi.org/10.1175/JPO-D-15-0193.1

Ivey, G. N., & Imberger, J. (1991). On the nature of turbulence in a stratified fluid. Part 1: The energetics of mixing. *Journal of Physical Oceanography*, *21*(5), 650–658. https://doi.org/10.1175/1520-0485(1991)021%3C0650:OTNOTI%3E2.0.CO;2

Ivey, G. N., Bluteau, G. N., & Jones, N. L. (2018). Quantifying Diapycnal Mixing in an Energetic Ocean. *Journal of Geophysical Research: Oceans*, *123*, 346–357. https://doi.org/10.1002/2017JC013242

Lozovatsky, I., & Fernando, H. J. (2013). Mixing efficiency in natural flows. *Philosophical Transactions of the Royal Society of London*, *A371*, 20120213, 20120213. https://doi.org/10.1098/rsta.2012.0213

Maffioli, A., Brethouwer, G., & Lindborg, E. (2016). Mixing efficiency in stratified turbulence. *Journal of Fluid Mechanics*, *794*, R3. https://doi.org/10.1017/jfm.2016.206

Mashayek, A., Salehipour, H., Bouffard, D., Caulfield, C. P., Ferrari, R., Nikurashin, M., et al. (2017). Efficiency of turbulent mixing in the abyssal ocean circulation. *Geophysical Research Letters*, *44*, 6296–6306. https://doi.org/10.1002/2016GL072452

Mead Silvester, J., Lenn, Y. D., Polton, J. A., Rippeth, T. P., & Morales Maqueda, M. (2014). Observations of a diapycnal shortcut to adiabatic upwelling of Circumpolar Deep Water along the Antarctic Continental Slope. *Geophysical Research Letters*, *41*, 7950–7956. https://doi.org/10.1002/2014GL061538

Nash, J. D., Kunze, E., Toole, J. M., & Schmitt, R. W. (2004). Internal tide reflection and turbulent mixing on the continental slope. *Journal of Physical Oceanography*, *34*(5), 1117–1134. https://doi.org/10.1175/1520-0485(2004)034%3C1117:ITRATM%3E2.0.CO;2

Osborn, T. R. (1980). Estimates of local rate of vertical dissipation measurements. *Journal of Physical Oceanography*, *10*(1), 83–89. https://doi.org/10.1175/1520-0485(1980)010%3C0083:EOTLRO%3E2.0.CO;2

Osborn, T. R., & Cox, C. S. (1972). Oceanic fine structure. *Geophysical and Astrophysical Fluid Dynamics*, *3*(1), 321–345. https://doi.org/10.1080/03091927208236085

Polzin, K.L. and Montgomery, E. T. (1998). Microstructure profiling with the high resolution profiler, Woods Hole Oceanographic Institution Technical Report, 16 pp.

Rohr, J., & van Atta, C. (1987). Mixing efficiency in stably stratified growing turbulence. *Journal of Geophysical Research*, *92*(C5), 5481–5488. https://doi.org/10.1029/JC092iC05p05481

Ruddick, B., Walsh, D., & Oakey, N. (1997). Variations in apparent mixing efficiency in the North Atlantic central water. *Journal of Physical Oceanography*, *27*(12), 2589–2605. https://doi.org/10.1175/1520-0485(1997)027%3C2589:VIAMEI%3E2.0.CO;2

Salehipour, H., & Peltier, W. R. (2015). Diapycnal diffusivity, turbulent Prandtl number and mixing efficiency in Boussinesq stratified turbulence. *Journal of Fluid Mechanics*, *775*, 464–500. https://doi.org/10.1017/jfm.2015.305

Salehipour, H., Peltier, W. R., Whalen, C. B., & MacKinnon, J. A. (2016). A new characterization of the turbulent diapycnal diffusivities of mass and momentum in the ocean. *Geophysical Research Letters*, *43*, 3370–3379. https://doi.org/10.1002/2016GL068184

Scotti, A., & White, B. (2016). The mixing efficiency of stratified turbulent boundary layers. *Journal of Physical Oceanography*, *46*(10), 3181–3191. https://doi.org/10.1175/JPO-D-16-0095.1

Shih, L. H., Koseff, J. R., Ivey, G. N., & Ferziger, J. H. (2005). Parameterization of turbulent fluxes and scales using homogenous sheared stably stratified turbulence simulations. *Journal of Fluid Mechanics*, *525*, 193–214. https://doi.org/10.1017/S0022112004002587

Smyth, W. D., Moum, J. N., & Caldwell, D. R. (2001). The efficiency of mixing in turbulent patches: Inferences from direct simulations and microstructure observations. *Journal of Physical Oceanography*, *44*, 1854–1872.

Squibb, M. E. (2014). Dynamics (Pembroke, Ont.) of shoaling internal waves in the near-shore: Mamala Bay, Hawaii. (PhD thesis). (167 pp.) Department of Civil and Environmental Engineering, Stanford University.

St. Laurent, L. C., & Schmitt, R. W. (1999). The contribution of salt fingers to vertical mixing in the North Atlantic Tracer Release Experiment. *Journal of Physical Oceanography*, *29*(7), 1404–1424. https://doi.org/10.1175/1520-0485(1999)029%3C1404:TCOSFT%3E2.0.CO;2

St. Laurent, L. C., Toole, J. M., & Schmitt, R. W. (2001). Buoyancy forcing by turbulence above rough topography in the Abyssal Brazil Basin. *Journal of Physical Oceanography*, *31*(12), 3476–3495. https://doi.org/10.1175/1520-0485(2001)031%3C3476:BFBTAR%3E2.0.CO;2

Street, R. L., Watters, G. Z., & Vennard, J. K. (1996). *Elementary fluid mechanics* (7th ed., p. 757). New York, NY: Wiley.

Toole, J. M., Polzin, K. L., & Schmitt, R. W. (1994). Estimates of diapycnal mixing in the abyssal ocean. *Science*, *264*(5162), 1120–1123. https://doi.org/10.1126/science.264.5162.1120

Turner, J. S. (1973). *Buoyancy effects in fluids*. Cambridge: Cambridge, UK. https://doi.org/10.1017/CBO9780511608827

Vennaygamoorthy, S. K., & Koseff, J. R. (2016). On the flux Rchardson number in stably stratified turbulence. *Journal of Fluid Mechanics*, *798*(R1), 1–10.

Walter, R. K., Squibb, M. E., Woodson, C. B., Koseff, J. R., & Monismith, S. G. (2014). Stratified turbulence in the nearshore coastal ocean: Dynamics and evolution in the presence of internal bores. *Journal of Geophysical Research: Oceans*, *119*, 8709–8730. https://doi.org/10.1002/2014JC010396

Waterhouse, A. F., MacKinnon, J. A., Nash, J. D., Alford, M. H., Kunze, E., Simmons, H. L., et al. (2014). Global patterns of diapycnal mixing from measurements of the turbulent dissipation rate. *Journal of Physical Oceanography*, *44*(7), 1854–1872. https://doi.org/10.1175/JPO-D-13-0104.1

Zhou, Q., Taylor, J. R., & Caulfield, C. P. (2017). Self-similar mixing in stratifed plane Couette flow for varying Prandtl number. *Journal of Fluid Mechanics*, *820*, 86–120.

Yamazaki, H., & Lueck, R. (1990). Why oceanic dissipation rates are not lognormal. *Journal of Physical Oceanography*, *20*(12), 1907–1918. https://doi.org/10.1175/1520-0485(1990)020%3C1907:WODRAN%3E2.0.CO;2